

Pattern formation and localization in the forced-damped FPU lattice

Ramaz Khomeriki^{1*}, Stefano Lepri^{1,2†}, Stefano Ruffo^{1,2,3‡}

¹*Dipartimento di Energetica “Sergio Stecco”*

Università di Firenze, Via S. Marta, 3 - I-50139 Firenze, Italy

² *Istituto Nazionale di Fisica della Materia, Unità di Firenze*

³ *Istituto Nazionale di Fisica Nucleare, Sezione di Firenze*

(November 10, 2018)

Abstract

We study spatial pattern formation and energy localization in the dynamics of an anharmonic chain with quadratic and quartic intersite potential subject to an optical, sinusoidally oscillating field and a weak damping. The zone-boundary mode is stable and locked to the driving field below a critical forcing that we determine analytically using an approximate model which describes mode interactions. Above such a forcing, a standing modulated wave forms for driving frequencies below the band-edge, while a “multibreather” state develops at higher frequencies. Of the former, we give an explicit approximate analytical expression which compares well with numerical data. At higher forcing space-time chaotic patterns are observed.

PACS numbers: 05.45.Jn; 05.45.Pq; 63.20.Pw; 63.20.Ry

I. INTRODUCTION

The dynamics of classical anharmonic lattices displays a rich variety of features. Already the simplest models, as the one-dimensional chain of equal-mass oscillators with nearest-neighbors nonlinear forces, exhibit nontrivial solutions like anharmonic waves [1,2], discrete

*Permanent address: Department of Physics, Tbilisi State University, Chavchavadze ave. 3, Tbilisi 380028, Georgia; e-mail: khomeriki@hotmail.com

†e-mail: lepri@avanzi.de.unifi.it

‡e-mail: ruffo@avanzi.de.unifi.it

solitons [3] and breathers [4]. Due to its simplicity, one of the most widely studied examples in this class is the celebrated Fermi-Pasta-Ulam (FPU) model [5], where the interparticle potential is a simple fourth-order polynomial in the relative displacements. Many investigations have focused on the process of energy equipartition among phonons, after having fed the energy into long wavelength modes, whose instability leads to the generation of solitons [6]. More recently the complementary case where the energy is placed into the highest frequency mode has been considered [7–9]. Above a certain energy threshold, which vanishes as $1/N$, N being the number of oscillators, this mode becomes modulationally unstable [11,12], leading to the growth of spatial modulations of the displacement field with a given finite wavelength. The subsequent evolution consists into the creation of localized structures (envelope solitons) which interact inelastically and coalesce in a few, large amplitude breathers [10]. These have however a finite lifetime and decay slowly until the asymptotic state of energy equipartition is attained.

Up to now, processes of this kind have been studied mainly for Hamiltonian lattices, and a quite natural question is to ask how such phenomena are affected by both forcing and/or dissipative mechanisms that may arise from the presence of an external field and of the interaction with other degrees of freedom, respectively. These issues were addressed by Rössler and Page [13], who found that localized modes can indeed exist in a sinusoidally driven, undamped FPU chain. More recently, the same authors performed detailed studies of the optical generation of such excitations under the action of suitable impulsive fields [14]. Later on, investigations of models of driven-damped antiferromagnetic chains [15] opened also the way to some experiments, whose outcomes are interpreted as manifestations of intrinsic localization [16]. Theoretical studies of the parametrically driven, discrete, nonlinear Schrödinger equation [18] and of coupled oscillator systems [17] have also been recently undertaken and led to the discovery of periodic, quasiperiodic and even chaotic breathers.

However, the relation between the phenomena observed in the Hamiltonian case with those appearing for forced-damped lattices has not yet been studied in detail. Indeed, we expect significant differences due to the creation of stationary states with nontrivial spatial structures, i.e. pattern formation [20,21]. In our context, having already studied the process of formation of stable localized structures arising from modulational instability in the conservative case [8], we are strongly motivated to see how the presence of forcing and damping affects this process. To remain close to the Hamiltonian case, we restrict ourselves to the case of small damping.

Various types of forcing are in principle possible, depending on the physical situation under study. However, a general requirement for localization is to excite band-edge modes. For Klein-Gordon lattices this is naturally realized using a spatially uniform driving field, which has been shown to induce interesting pattern formation phenomena [19]. On the other hand, this forcing would be ineffective for FPU lattices, because, due to the symmetry of the Hamiltonian, the zero mode is decoupled (see below). Alternatively, since spatial localization appears from the instability of band-edge modes, we choose in this paper to drive the system at the zone boundary wavelength. Moreover, we consider the simplest case

in which the driving field oscillates sinusoidally in time.

In Section II we introduce the model and further comment on some of its features. After introducing a specific mode expansion of the displacement field, we obtain approximate equations of motion for such modes in the weak damping limit. Some details of the numerical simulations are presented as well as the quantities used to detect localization and to study spectral properties.

Section III deals with the full characterization of the weak forcing solution where the zone boundary mode is locked to the driving field. By increasing the forcing parameter such a solution becomes unstable. Approximate values of the critical forcing and frequency are analytically computed and successfully compared with numerical results.

Just beyond this instability more complex spatial patterns are attained by the system. For small enough frequencies a stable standing wave arises, which we describe analytically by solving for the fixed point of a suitable truncated mode expansion (Section IV). When the driving frequency exceeds a given resonant value a multibreather, spatially aperiodic state is instead observed in numerical simulations (Section V).

Section VI is devoted to some conclusions and to a brief discussion of the transition to chaos, which is observed by increasing the forcing.

II. THE FORCED AND DAMPED FPU MODEL

The equations of motion of forced-damped FPU oscillator chain are

$$\ddot{u}_n = u_{n+1} + u_{n-1} - 2u_n + (u_{n+1} - u_n)^3 + (u_{n-1} - u_n)^3 - \gamma \dot{u}_n + f \cos(\omega t - \pi n), \quad (1)$$

where u_n denotes the displacement of n -th oscillator with respect to its equilibrium position. Periodic boundary conditions, $u_{n+N} = u_n$, are assumed, with N being the number of oscillators. Dimensionless units are used such that the masses, the linear and nonlinear force constants and the lattice spacing are taken equal to unity. The forcing and damping strengths are gauged by the parameters f and γ , respectively, and ω is the driving frequency. As already mentioned in the Introduction, the choice of the forcing with the shortest wavelength is expected to favour the growth of localized excitations. Physically, the last term in Eq. (1) models the interaction of a uniform electric field applied to a chain of alternating opposite charges; it can in fact be written as $f(-1)^n \cos \omega t$ [13]. Let us stress again that the more widely studied case of uniform forcing [19] is not viable for models like (1), because the zero mode is completely decoupled from the others as a consequence of the invariance of (1) under the transformation $u_n \rightarrow u_n + \text{const}$.

In order to describe the forced oscillations of the system it is convenient to represent the displacement field in the form

$$u_n = \frac{1}{2} \sum_k \left[a_k e^{i(\omega t + kn)} + a_{-k}^+ e^{-i(\omega t - kn)} \right], \quad (2)$$

where a_k are complex mode amplitudes and $-\pi < k \leq \pi$ the corresponding wavenumber. Throughout the paper we will mainly focus our attention on the dynamics of the zone-boundary mode, which we refer to as π -mode for the sake of brevity.

The equations of motion for the amplitudes a_k 's are obtained by substituting Eq. (2) into Eq. (1). Similarly to what is done for the undamped case [4], a considerable simplification is achieved by neglecting higher-order harmonics that are produced by the cubic terms (the so-called rotating wave approximation). Moreover, in the limit of weak damping $\gamma \ll \omega$ we find the following set of approximate equations

$$-2i\omega\dot{a}_k - i\omega\gamma a_k = (\omega_k^2 - \omega^2)a_k + \delta_{k,\pi}f + 6 \sum_{q_1, q_2} G_{q_1, q_2}^k a_{q_1} a_{q_2} a_{q_1+q_2-k}^+, \quad (3)$$

where $\omega_k^2 = 2(1 - \cos k)$, $\delta_{k,\pi}$ is equal to one for $k = \pi$ and zero otherwise and

$$G_{q_1, q_2}^k = \frac{1}{4} [1 + \cos(q_1 + q_2) + \cos(k - q_2) + \cos(k - q_1) - \cos k - \cos q_1 - \cos q_2 - \cos(k - q_1 - q_2)].$$

Eqs. (3) correspond to the positive frequency projection in the base given in Eq. (2), the negative frequency ones being obtained by replacing $k \rightarrow -k$ and taking the complex conjugate.

In the following, we aim at comparing the analytical predictions that can be drawn from the set of approximate equations (3) with the direct numerical simulations of model (1). We have integrated the equations of motion (1) by means of a fourth-order Runge-Kutta algorithm with a step ranging between 10^{-2} and 10^{-3} . We have always chosen an initial condition with all oscillators in their equilibrium position $u_n(0) = 0$ and small (of the order of 10^{-5}) random Gaussian distributed initial velocities $\dot{u}_n(0)$. Several series of simulations have been performed for different values of the parameters ω and f and for fixed $\gamma = 0.1$. The latter choice guarantees that the condition $\gamma \ll \omega$ holds in the resonance regions close to the band-edge, i.e. $|\omega| \sim \omega_\pi = 2$ which is of main interest here. Furthermore, the resulting time-scales are reasonably short to allow a real-time analysis for chains as long as $N = 512$. Nonetheless, some of the results reported below have been checked also for another series of simulations performed with $\gamma = 0.01$.

We have monitored the energy density along the chain

$$h_n = \frac{1}{2}\dot{u}_n^2 + \frac{1}{2} [(u_{n+1} - u_n)^2 + (u_n - u_{n-1})^2] + \frac{1}{4} [(u_{n+1} - u_n)^4 + (u_n - u_{n-1})^4], \quad (4)$$

as well as the spectrum of mode energies

$$\varepsilon_k = |\dot{U}_k|^2 + \omega^2 |U_k|^2 \quad (5)$$

where

$$U_k = \frac{1}{\sqrt{N}} \sum_{n=1}^N u_n e^{ikn} = \frac{\sqrt{N}}{2} (a_k e^{i\omega t} + a_{-k}^+ e^{-i\omega t}) \quad (6)$$

is the amplitude of the k -th Fourier mode, which can be efficiently computed using a standard FFT routine. In the limit in which the a_k 's are slowly varying with respect to the forcing or reach a stationary value, one finds that $\varepsilon_k = N\omega^2|a_k|^2$ is constant in time. On the other hand, when monitoring quantities like h_n and/or u_n it is convenient to observe the system at time intervals that are integer multiples of the driving period.

III. MODULATIONAL INSTABILITY OF THE π -MODE

Let us begin by considering solutions where only the π mode is excited. Such solutions are numerically observed to exist and be stable below a certain critical forcing f_{cr} that depends on both ω and γ . Indeed, in the typical simulation described at the end of the previous Section, all modes with $k \neq \pi$ damp out on a time-scale set by the value of γ while $|a_\pi|$ rapidly grows and finally approaches a constant value. Such asymptotic amplitude a_π is obtained by solving for the stationary solution of Eqs. (3), which corresponds to an oscillation locked to the driving field with a constant phase lag. We get

$$a_\pi = \frac{f}{\omega^2 - 4 - 12|a_\pi|^2 - i\gamma\omega} \quad , \quad (7)$$

and writing $a_\pi = |a_\pi| \exp(i\theta_\pi)$ one gets

$$\theta_\pi = \text{atan} \left(\frac{\gamma\omega}{\omega^2 - 4 - 12|a_\pi|^2} \right) \quad , \quad (8)$$

where the squared modulus $z = |a_\pi|^2$ is the solution the cubic equation

$$144z^3 - 24(4 - \omega^2)z^2 + [(4 - \omega^2)^2 + \gamma^2\omega^2]z = f^2 \quad . \quad (9)$$

One can easily ascertain that the latter admits a single real root only for $|\omega| < \omega_*$ where $\omega_* \simeq 2 + \sqrt{3}\gamma/2$, while three distinct roots may otherwise exist (see the discussion in the following).

Before treating in detail the differences between the two cases, let us address the question of stability. This is accomplished by solving the set of equations obtained linearizing Eqs. (3) around the stationary solutions (i.e. neglecting all interaction terms which are nonlinear in the a_{ks})

$$-2i\omega\dot{a}_k - i\omega\gamma a_k = (\tilde{\omega}_k^2 - \omega^2)a_k + 3\omega_k^2 a_\pi^2 a_{-k}^+ \quad , \quad (10)$$

where

$$\tilde{\omega}_k^2 = (1 + 6|a_\pi|^2)\omega_k^2 \quad (11)$$

is the frequency of the k -th mode shifted by the interaction with the π -mode. As usual, Eq. (10), together its complex conjugate, are solved looking for solutions of the form $\exp(\nu_k t)$. The relevant branch of the eigenvalue spectrum reads

$$\nu_k = -\frac{\gamma}{2} + \frac{1}{2|\omega|} \sqrt{9\omega_k^4 |a_\pi|^4 - (\tilde{\omega}_{k_*}^2 - \omega^2)^2}. \quad (12)$$

The growth rate $Re\{\nu_k\}$ is maximal when the square root in the above expression attains its maximum value, i.e. when the resonance condition $\omega = \tilde{\omega}_{k_*}$ holds [22]. The latter, together with definition (11), fixes the value of the wavenumber k_* of the most unstable mode as

$$\cos k_* = 1 - \frac{\omega^2}{2(1 + 6|a_\pi|^2)}. \quad (13)$$

In the case in which a single real root of (9) exists (i.e. $|\omega| < \omega_*$), the threshold for modulational instability can be computed explicitly. Indeed, by letting $\nu_k = 0$ in Eq. (12) and using formula (13), one gets

$$|a_\pi|_{cr}^2 = \frac{\gamma}{3(\omega - 2\gamma)}. \quad (14)$$

Finally, from formula (7) one derives the value of the critical forcing

$$f_{cr} = \sqrt{\frac{\gamma}{3(\omega - 2\gamma)} \left\{ \left[\omega^2 - \frac{4(\omega - \gamma)}{\omega - 2\gamma} \right]^2 + \gamma^2 \omega^2 \right\}}. \quad (15)$$

In the case where three solutions exist ($|\omega| > \omega_*$), the stability properties must be considered separately for each of them. Let us discuss this issue with reference to the case $\omega = 2.4$, illustrated by the graph in Fig. 1. Here the three solutions, which we label A, B and C, coexist in the range $f_+ < f < f_-$. The values of f_\pm can be computed from Eq. (9), since they correspond to the amplitudes

$$|a_\pi^\pm|^2 = \frac{2(\omega^2 - 4) \pm \sqrt{(\omega^2 - 4)^2 - 3\gamma^2 \omega^2}}{36}. \quad (16)$$

Hence, from formula (7) we obtain

$$f_\pm = |a_\pi^\pm| \sqrt{(\omega^2 - 4 - 12|a_\pi^\pm|^2) + \gamma^2 \omega^2}. \quad (17)$$

Looking at the spectrum (12), it turns out that the largest amplitude solution C is always modulationally unstable. The intermediate amplitude solution B is modulationally unstable above $|a_\pi|^2 = (\omega^2 - 4)/24$ (corresponding to $f = 0.235$ in Fig. 1) while it has the maximal growth rate at $\pm\pi$ below this point. The smaller amplitude solution A is instead found to be always stable. Since we choose to run the dynamics starting always with almost zero mode amplitudes, it would be natural to conclude that the resulting trajectory converges to the solution A up to its existence boundary and hence that $f_{cr} = f_-$. The numerical simulations show that this conclusion is not actually correct. Indeed, the system approaches the stable solution A only up to a critical value of the forcing f_{cr}^{int} which is definitely smaller than f_- (see the diamonds in Fig. 1). Beyond such a value, the π -mode undergoes modulational instability similar to the previous case.

An interpretation of this phenomenon can be given in the following way. Let us consider the equations of motion for the “internal” dynamics of the π -mode that can be derived from Eq. (3),

$$-2i\omega\dot{a}_\pi - i\omega\gamma a_\pi = (4 - \omega^2)a_\pi + f + 12a_\pi|a_\pi|^2. \quad (18)$$

This nonlinear equation provides a good approximation of the dynamics as long as all the other modes are not significantly excited. Its numerical solution indicates that for $f = f_{cr}^{int}(\omega)$ the initial condition $a_\pi(0) = 0, \dot{a}_\pi(0) = 0$ exits the basin of attraction of the fixed point corresponding to the solution A. Such a value corresponds pretty well to the actual critical forcing numerically determined for the full system (see the solid vertical line at f_{cr}^{int} in Fig. 1). In other words, at f_{cr}^{int} the dynamics leaves the lowest amplitude solution A because of this internal instability and “jumps” into the modulationally unstable region. Since a fixed point will not be subsequently approached, we do not expect that the corresponding spectrum of growth rates will be described by formula (12). Nonetheless, a reasonable qualitative agreement between the two is observed, being both characterized by a sharp maximum around the most unstable mode with some broadened band around it.

Finally, the results described above are summarized in Fig. 2, where we show the control parameter space (f, ω) . The dashed line for $|\omega| < \omega_*$ is the theoretical expression (15) for the modulational instability valid when only one solution is present. At ω_* two full lines start, given by formula (17), which bound the region where three solutions occur. Inside this region, the dotted line f_{cr}^{int} is the one obtained numerically by looking at the internal π -mode instability, as we have described above. The numerical data (full triangles) were obtained by looking at the incipient modulational instability of the full system. An excellent agreement (within some percent) with the theoretical results is observed in the considered frequency range. We have also checked that the critical wavenumber k_* is accurately predicted by Eq. (13). We thus conclude that both the theory developed for the case of one solution and the approximate description of the internal instability when three solution are present are basically correct.

IV. STANDING NONLINEAR WAVES

Let us now describe the states forming just above the threshold f_{cr} , after the development of the modulational instability. Two different behaviors appear depending whether the driving frequency lies below or above a resonance frequency, which for small γ is very close to the upper band edge $\omega \simeq 2$. In this Section we discuss the first case. As expected from the spectrum (12), the development of the instability leads to a fast growth of the modes belonging to the unstable band around k_* (and also its harmonics, see below). Afterwards, the main band shrinks until the system saturates to the asymptotic state. The result is basically a modulated standing wave locked in time with the forcing field (see the example illustrated in Fig. 3) and the wavenumber of the modulation is indeed very close to the expected value $\pi - k_*$ with k_* given by Eq. (13). Furthermore, this state appears to be

stable, at least on the time scale considered in the simulations. For instance, the wave profile shown in Fig. 3 remains unaltered up to $2 \cdot 10^5$ time units, i.e. for more than $6 \cdot 10^4$ driving periods.

An approximate theoretical analysis can explain the formation of this pattern. Indeed, in view of the above results, it is reasonable to look for a simplified description that neglects all the modes but the π -mode and the most unstable one with wavenumber k_* . Under such assumptions and taking into account the resonance condition we obtain from Eqs. (3) the following coupled equations for a_π and a_{k_*} :

$$\begin{aligned} -2i\omega\dot{a}_\pi - i\omega\gamma a_\pi &= (4 - \omega^2)a_\pi + f + 12a_\pi|a_\pi|^2 + 6\omega_{k_*}^2 a_\pi^+ a_{k_*} a_{-k_*} + 12\omega_{k_*}^2 a_\pi |a_{k_*}|^2. \\ -2i\omega\dot{a}_{k_*} - i\omega\gamma a_{k_*} &= 3\omega_{k_*}^2 a_\pi^2 a_{-k_*}^+ + \frac{9}{4}\omega_{k_*}^4 a_{k_*} |a_{k_*}|^2 \quad . \end{aligned} \quad (19)$$

The first equation is nothing but the modified version of Eq. (18) with the interaction terms between π and k_* modes included. The stationary solutions are determined letting $a_{k_*} = |a_{k_*}| \exp(i\theta_{k_*})$ and first solving the second of Eqs. (19)

$$|a_{\pm k_*}|^2 = \frac{4}{3\omega_{k_*}^2} \sqrt{|a_\pi|^4 - |a_\pi|_{cr}^4}, \quad \sin 2(\theta_\pi - \theta_{\pm k_*}) = -\frac{|a_\pi|_{cr}^2}{|a_\pi|^2} \quad . \quad (20)$$

Substituting the latter in the first of Eqs. (19) we get the stationary value of $|a_\pi|$ above threshold

$$\begin{aligned} |a_\pi|^2 \left[\left(\omega^2 - 4 - 12|a_\pi|^2 - 16\sqrt{|a_\pi|^4 - |a_\pi|_{cr}^4} + 8\frac{|a_\pi|^4 - |a_\pi|_{cr}^4}{|a_\pi|^2} \right)^2 + \right. \\ \left. \left(\gamma\omega + 8\sqrt{|a_\pi|^4 - |a_\pi|_{cr}^4} \right)^2 \right] = f^2, \end{aligned} \quad (21)$$

Solving this equation, we can thus get $|a_{\pm k_*}|$ and $\theta_{\pm k_*}$ from Eq. (20). A fourth equation, which we do not explicitly display here for the sake of brevity, allows to compute θ_π as well.

The stationary solution obtained above corresponds to a displacement field which can be derived using expansion (2)

$$u_n = |a_\pi|(-1)^n \cos(\omega t + \theta_\pi) + 2|a_{k_*}| \cos(k_* n) \cos(\omega t + \theta_{k_*}) \quad , \quad (22)$$

which is precisely a standing modulated wave. These analytical results are also in reasonable quantitative agreement with numerical data. For example, in the case of Fig. 3 ($\omega = 1.8$, $f = 0.150$ and $\gamma = 0.1$) we get

$$|a_\pi|^2 = 0.02085 \quad |a_{k_*}|^2 = 4.88 \cdot 10^{-4} \quad (\text{numerical}) \quad (23)$$

$$|a_\pi|^2 = 0.02085 \quad |a_{k_*}|^2 = 4.27 \cdot 10^{-4} \quad (\text{theoretical}) \quad , \quad (24)$$

the relative deviations being as expected of the order γ/ω .

The above expressions are simplified close to threshold and sufficiently far from resonance. Indeed in this case θ_π is vanishingly small (see Eq. (8)) and therefore one gets, from formulas (20), $\theta_{k_*} \simeq \pi/4$ and the approximate solution

$$u_n \simeq |a_\pi|(-1)^n \cos(\omega t) + 2|a_{k_*}| \cos(k_* n) \cos(\omega t + \frac{\pi}{4}) \quad . \quad (25)$$

This solution compares well with numerical data. Looking at the pattern at times which are integer multiples of $2\pi/\omega$, again for the example of Fig. 3 with the values in formula (24).

$$\begin{aligned} u_n &\simeq 0.1437(-1)^n + 0.0292 \cos(2.05n) \quad (\text{theoretical}) \\ u_n &= 0.142(-1)^n + 0.0359 \cos(2.025n) \quad (\text{numerical}) \quad , \end{aligned} \quad (26)$$

which shows a good agreement.

Before concluding this Section, let us discuss the issue of higher-order corrections to the solution (22). Indeed, besides the main component at k_* , the nonlinear terms induce the presence of several (exponentially small) harmonics whose wavenumber can be expressed as (recall that $-\pi < k \leq \pi$)

$$k_n = k_* n + (n - 1)\pi, \quad n = 2, 3, \dots \quad (27)$$

Their amplitudes can be computed perturbatively from the stationary solution of Eq. (3). For instance, the first harmonic ($n = 2$) is evaluated as a function a_π and a_{k_*} . We give here for completeness the explicit expressions of the first and second harmonics.

$$|a_{k_2}| = \frac{18 \cos k_* (\cos k_* - 1)}{\omega_{k_2}^2 - \omega^2} |a_\pi| |a_{k_*}|^2, \quad (28)$$

$$|a_{k_3}| = \frac{3|1 - 6 \cos^2 k_* + 2 \cos^3 k_*|}{|\omega_{k_3}^2 - \omega^2|} |a_{k_*}|^3. \quad (29)$$

Higher-order harmonics ($n > 2$) can be thus computed recursively in a similar way obtaining the general result

$$a_{k_n} = \frac{6}{\omega_{k_n}^2 - \omega^2} \sum_{q_n, p_n, r_n < k_n} G_{q_n, p_n}^{k_n} a_{q_n} a_{p_n} a_{-r_n}^+, \quad q_n + p_n + r_n = k_n. \quad (30)$$

Notice that an infinite number of harmonics is expected here. This shows that the waves we are dealing with are more general than those previously reported in the literature for damped-driven Klein-Gordon lattices [19]. In this latter case, the modulation has a finite number of harmonics due to the peculiar mutual relationship among modes 0 , $\pi/2$ and π that allows for solution where no other modes are excited.

V. MULTIBREATHING STATES

A different scenario is observed for driving frequency above resonance, which we briefly describe here with reference to the case $\omega = 2.4$, illustrated in Fig. 4. The instability described at end of Section III produces, on a relatively short time scale ($t \sim 10^2$), a disordered assembly of sharply localized structures in a similar way to what is observed for the undriven case [8,10]. On longer time scales ($t \sim 10^3$), a further stage follows in which

the localized peaks arrange themselves until they eventually reach an asymptotic state (see the upper panel of Fig. 4). This is a sort of “multibreather” state, i.e. an array of *unevenly spaced* breathers. Remarkably, such a complex solution appears to be stable as the previously illustrated nonlinear wave. For instance, the pattern in Fig. 4 has been observed to persist up to a time $2.0 \cdot 10^5$, i.e. more than $7 \cdot 10^4$ driving periods.

The corresponding displacement field in Fig. 5 reveals that each breather is pretty similar to the “even-parity” localized modes found in the Hamiltonian case [12], the main difference being the presence of a π -mode background induced by the field. No “odd-parity” mode is generated by the above mechanism in all the examined cases. Actually, a closer inspection reveals that two distinct solutions of slightly different amplitude are present. Moreover, apart from a small lag induced by the damping, the background oscillates always out of phase with respect to the field as it can be ascertained by comparing the dotted line in Fig. 5 with the corresponding displacement pattern. On the contrary, the breathers are always in-phase with the field. Accordingly, depending on the site on which they sit, they can have equal or opposite relative phases. Although localized solutions oscillating out of phase with the field are known to exist in similar models [13], they are not detected in the present context.

The inhomogeneous distribution of vibrational energy is distinctly reflected in the mode spectrum (see the lower panel of Fig. 4), which displays a localized structure and a band broadening as a consequence of the irregular spacing among the breathers.

To give a more firm basis to our numerical observations, it is useful to briefly point out some conclusions that can be drawn by a suitable continuum approximation of the FPU model. In analogy with the approach followed for the hamiltonian case [10], one can in fact write the displacement field as $u_n = (-1)^n Re\{\psi(x, t) \exp(i\omega t)\}$ where ψ is an envelope function which is assumed to be slowly varying in space and time on scales of the order of the interatomic spacing and the driving period, respectively. A standard calculation leads to the driven-damped nonlinear Schrödinger equation

$$2i\omega\dot{\psi} + (4 - \omega^2 + i\omega\gamma)\psi + \psi_{xx} + 12\psi|\psi|^2 = f \quad , \quad (31)$$

which in the spatially uniform case reduces to Eq. (18) for the π -mode amplitude. Notice however that this type of description makes sense only when a relatively narrow packet of modes close to $\pm\pi$ is excited and is thus less general than the one based on Eqs. (3). For a suitable choice of parameters, Eq. (31) admits two soliton solutions of different amplitudes [23] as well as stable multisoliton complexes arising from bifurcation of one of them [24]. Thus, the localized states of Fig. 5 could be related to such solutions, at least to the extent in which our lattice model can be approximated by a continuum equation like (31). Although a more quantitative comparison would be desirable, this is a solid argument in support of the existence of stable multibreather complexes.

VI. CONCLUSIONS AND PERSPECTIVES

We have confirmed that modulational instability of zone boundary modes is a relevant mechanism for the generation of nontrivial spatial structures in discrete anharmonic lattices. Our results for the externally driven case complement previous studies on Hamiltonian models and further show that the interplay of (almost) resonant forcing and damping can stabilize such structures. Our approximate analytical framework has allowed also to derive the stability chart of the zone-boundary mode. For forcing frequencies below resonance a modulated wave is formed after instability, whose approximate analytical expression we have derived in terms of mode amplitudes. For frequencies above resonance a “multibreather” state arises of which we have given a phenomenological characterization. There are other problems that could be attacked within this approach, like the interesting issue of destabilization of the modulated wave. This could also contribute to a better understanding of localization mechanisms. Furthermore, this points out the possibility of generating long-living and complex energy distributions in space for real ionic crystals under the action of optical fields.

Let us also briefly comment on the fate of the two typical spatial patterns described above. As expected, increasing the forcing leads to their destabilization and eventually to the transition to chaos (see the stars in Fig. 2 as well as Fig. 6). This bears a strong analogy with the *parametrically* driven-damped nonlinear Schrödinger equation where stable patterns precede the onset of chaotic behavior [25]. This is a further indication that a considerable insight on the dynamics of the discrete model may be achieved from Eq. (31). Besides of this, it has been suggested on quite general grounds that systems obeying the symmetry $u_n \rightarrow u_n + \text{const.}$ should show an abrupt transition to a soft-turbulent state without displaying any intermediate spatial pattern [26]. This is in apparent contradiction with the existence of stable patterns found in our numerics. On the other hand, performing simulations at $\gamma = 0$ the transition to chaos occurs as soon as $f \neq 0$, since the modulational pattern does not attain any regular asymptotic state. We can therefore conjecture that the presence of friction alters the nature of the transition in a way that remains to be understood.

ACKNOWLEDGMENTS

We acknowledge useful discussions with the members of the research group *Dynamics of Complex Systems* in Florence as well as a partially support by the INFM project *Equilibrium and nonequilibrium dynamics in condensed matter*. This work is also part of the EC network LOCNET, Contract No. HPRN-CT-1999-00163 and of the MURST-COFIN00 project “Chaos and localization in classical and quantum mechanics”. R. Kh. is obliged to CNR-NATO for the visiting scientist fellowship award providing the financial support for his stay in Florence University.

REFERENCES

- [1] Yu. A. Kosevich, Phys. Rev. Lett. **71**, 2058 (1993).
- [2] P. Poggi, S. Ruffo, Physica D **103**, 251 (1997).
- [3] N. Flytzanis, S. Pneumatikos, M. Peyrard, J. Phys. A **22** 783 (1989).
- [4] S. Flach, C.R. Willis, Phys. Rep., **295**, 181, (1998).
- [5] E. Fermi, J. Pasta, S. Ulam, M. Tsingou, in *The Many-Body Problems*, edited by D.C. Mattis (World Scientific, Singapore, 1993 reprinted).
- [6] A.J. Lichtenberg, M.A. Lieberman, *Regular and Chaotic Dynamics*, Springer, Berlin, (1992), Chapt. 6.5.
- [7] V.M. Burlakov and S.A. Kiselev, Zh. Eksp. Teor. Fiz. **99**, 1526 (1991) [Sov. Phys. JETP **72**, 854 (1991)].
- [8] T. Cretegny, T. Dauxois, S. Ruffo, A. Torcini, Physica D, **121**, 109, (1998).
- [9] K. Ullmann, A.J. Lichtenberg, G. Corso, Phys. Rev. E, **61** 2471 (2000); V.V. Mirnov, A.J. Lichtenberg, H. Guclu (unpublished).
- [10] Yu. A. Kosevich and S. Lepri, Phys. Rev. B, **61** , 299 (2000).
- [11] I. Daumont, T. Dauxois, M. Peyrard, Nonlinearity, **10**, 617, (1997).
- [12] K.W. Sandusky, J.B. Page, Phys. Rev. B, **50**, 866, (1994).
- [13] T. Rössler, J.B. Page, Phys. Lett. A., **204**, 418, (1995)
- [14] T. Rössler, J.B. Page, Phys. Rev. Lett., **78**, 1287, (1997); Phys. Rev. B **62**, 11460 (2000)
- [15] R. Lai, A.J. Sievers, Phys. Rev. Lett. **81** 1937 (1998).
- [16] U. T. Schwarz, L.Q. English, A.J. Sievers, Phys. Rev. Lett. **83** 223 (1999).
- [17] P.J. Martínez, L.M. Floría, F. Falo and J.J. Mazo, Europhys. Lett **45** 444 (1999).
- [18] D. Hennig, Phys. Rev. E., **59**, 1637, (1999).
- [19] V.M. Burlakov, Phys. Rev. Lett., **80**, 3988, (1998).
- [20] V.S. L'vov, *Nonlinear Spin Waves*, Nauka, Moscow, (1983).
- [21] P. Manneville, *Dissipative structures and weak turbulence*, Academic Press, Boston (1990).
- [22] Notice that this resonance condition is actually approximate. Indeed, upon setting to zero the derivative of ν_k with respect to k , one finds it to be valid up to a small

correction (of order $|a_\pi|^4$) which we neglect for the sake of simplicity in deriving the analytical solution.

- [23] I.V. Barashenkov, Yu. S. Smirnov, Phys. Rev. E., **54** 5707 (1996).
- [24] I.V. Barashenkov, Yu. S. Smirnov, N.V. Alexeeva, Phys. Rev. E., **57** 2350 (1998).
- [25] M. Bondila, I. V. Barashenkov and M. M. Bogdan Physica D, **87** 2350 (1995).
- [26] M.I. Tribelsky, Usp. Fiz. Nauk, **167**, 167, (1997) [Phys. Usp. **40**, 159, (1997)].

FIGURES

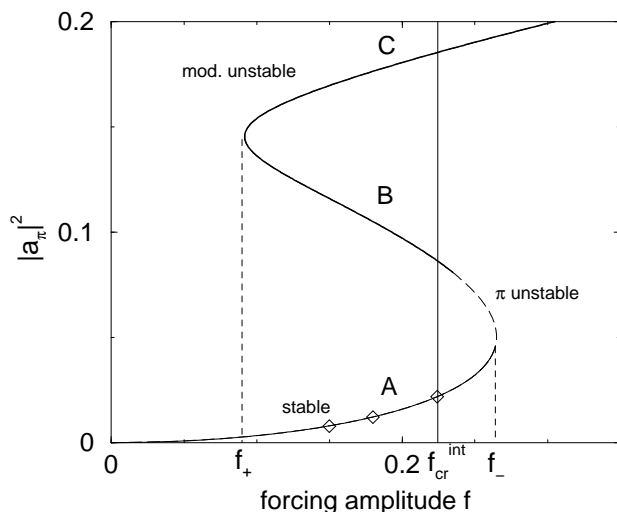


FIG. 1. Squared amplitude of the multiple fixed-point solutions vs. the forcing f for $\omega = 2.4$ and $\gamma = 0.1$. The solid vertical line represents the critical value of the forcing $f_{cr}^{int} = 0.224$. Dashed lines are the boundaries for the range $f_+ < f < f_-$ where three solutions exist. The letters A,B,C denote the three solutions from the smallest to the highest amplitude one.

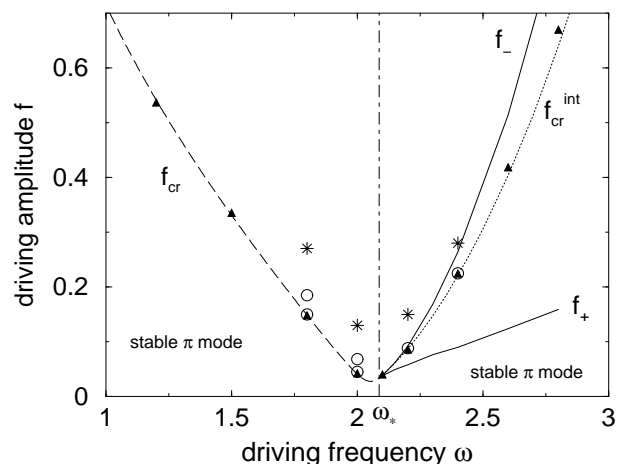


FIG. 2. Control parameter plane (ω, f) for $\gamma = 0.1$. The dashed line for $\omega < \omega_*$ is the critical forcing f_{cr} given by formula (15) at which modulational instability occurs. The region for $\omega > \omega_*$ where three solutions exist is bounded by the solid lines f_{\pm} . The dotted line within corresponds to the instability threshold f_{cr}^{int} evaluated numerically from Eq. (18). The full triangles are the numerical estimates of f_{cr} . Open circles left (resp. right) of the $\omega = \omega_*$ line denote points where standing waves (resp. breathers) occur. The stars are some parameter values for which chaos is detected.

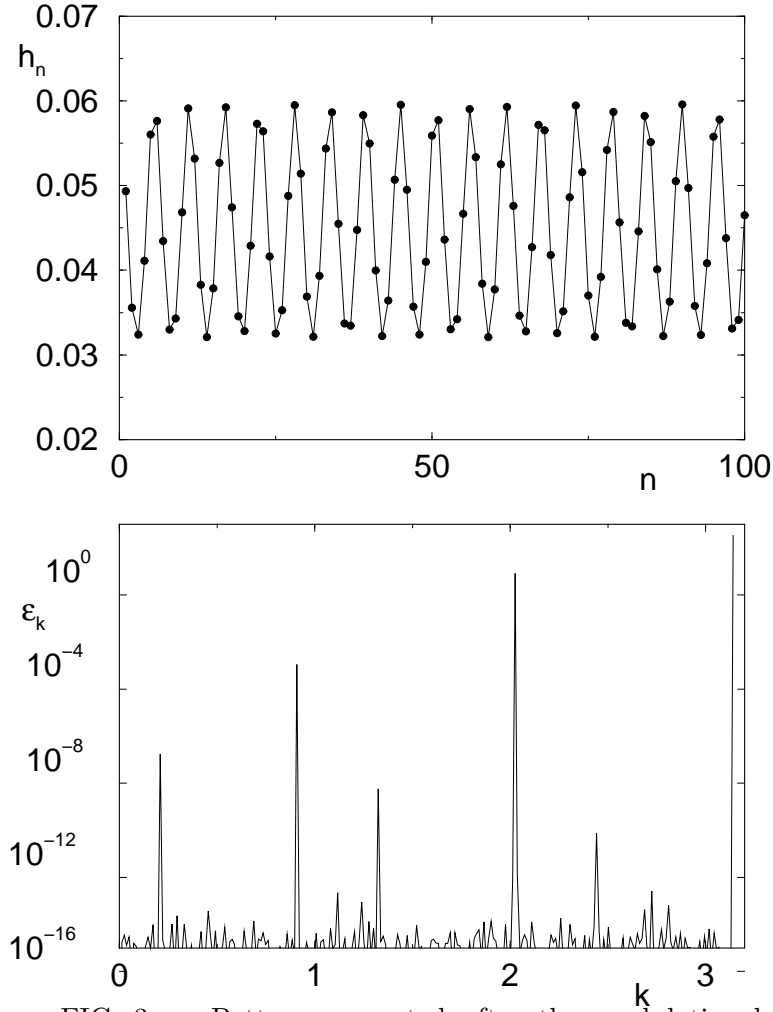


FIG. 3. Pattern generated after the modulational instability for $\omega = 1.8$, $f = 0.150$ ($f_{cr} = 0.148$). This pattern stabilizes at $t \simeq 10^4$. In the upper panel we show the energy density in a part of a chain of 512 particles, in the lower the corresponding mode energy spectrum in lin-log scale.

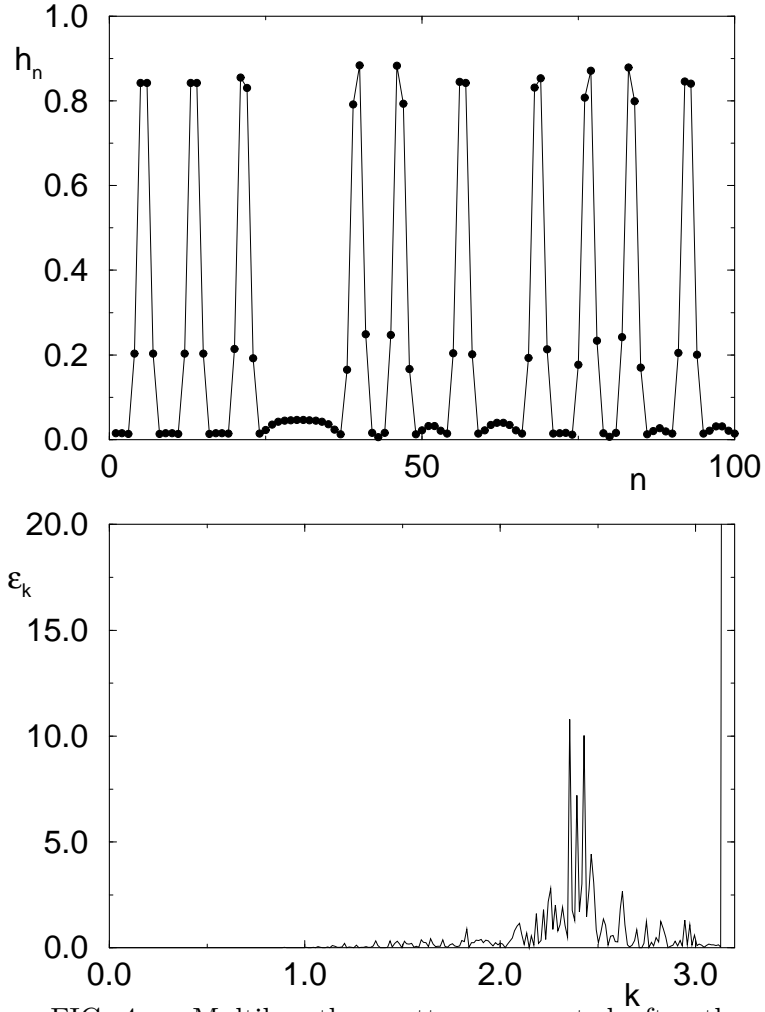


FIG. 4. Multibreather pattern generated after the modulational instability for $\omega = 2.4$, $f = 0.2250$ ($f_{cr} = 0.2245$). This pattern stabilizes at $t \simeq 5 \cdot 10^3$. In the upper panel we report the energy density, in the lower the mode energy spectrum.

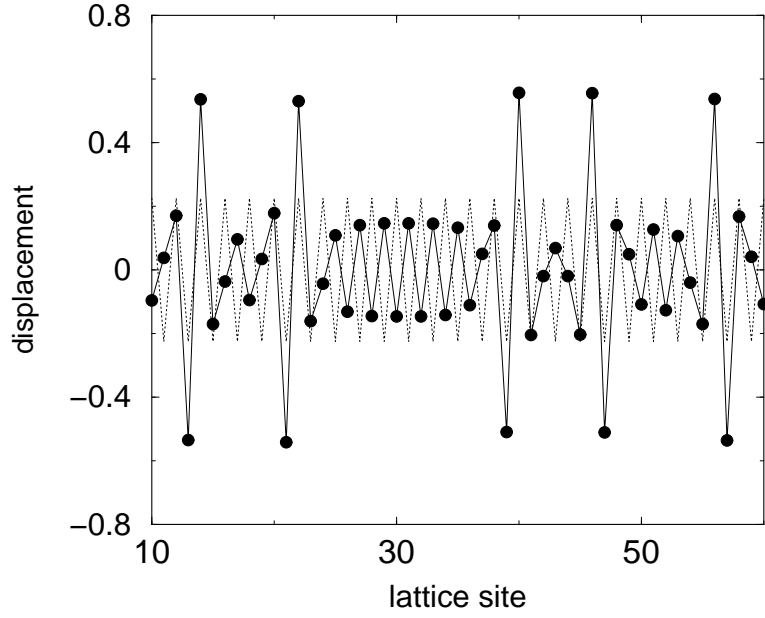


FIG. 5. Displacement pattern corresponding to the case of Fig. 4. The dashed line is the instantaneous configuration of the driving field showing relative phase relations.

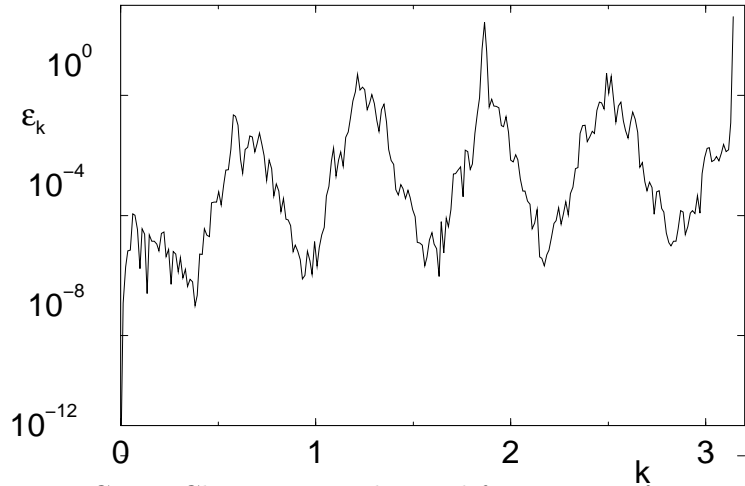
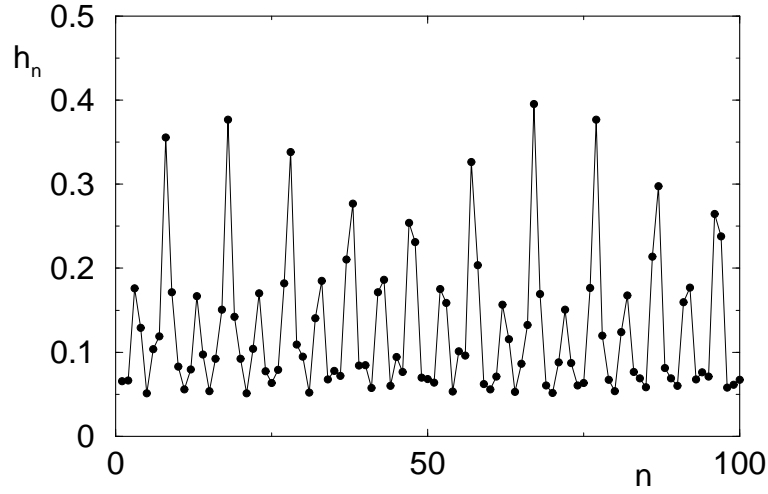


FIG. 6. Chaotic state obtained for $\omega = 1.8$, $f = 0.27$. In the upper panel we show a snapshot of the energy density along the chain at $t = 5200$ and in the lower the corresponding mode energy spectrum in lin-log scale.